



Cite this: *Lab Chip*, 2016, 16, 3788

Dielectric elastomer actuator for mechanical loading of 2D cell cultures†

Alexandre Poulin,^{*a} Cansaran Saygili Demir,^b Samuel Rosset,^a Tatiana V. Petrova^b and Herbert Shea^a

We demonstrate the use of dielectric elastomer actuators (DEAs) for mechanical stimulation of cells *in vitro*. The development of living tissues is regulated by their mechanical environment through the modification of fundamental cellular functions such as proliferation, differentiation and gene expression. Mechanical cues have been linked to numerous pathological conditions, and progress in cellular mechanobiology could lead to better diagnosis and treatments of diseases such as atherosclerosis and cancers. Research in this field heavily relies on *in vitro* models due to the high complexity of the *in vivo* environment. Current *in vitro* models however build on bulky and often complex sets of mechanical motors or pneumatic systems. In this work we present an alternative approach based on DEAs, a class of soft actuators capable of large deformation (>100%) and fast response time (<1 ms). The key advantage of DEAs is that they can be integrated within the culture substrate, therefore providing a very compact solution. Here we present a DEA-based deformable bioreactor which can generate up to 35% uniaxial tensile strain, and is compatible with standard cell culture protocols. Our transparent device also includes a static control area, and enables real-time optical monitoring of both the stimulated and control cell populations. As a proof of concept we cycled a population of lymphatic endothelial cells (LECs) between 0% and 10% strain at a 0.1 Hz frequency for 24 h. We observe stretch-induced alignment and elongation of LECs, providing the first demonstration that DEAs can be interfaced with living cells and used to control their mechanical environment.

Received 17th July 2016,
Accepted 17th August 2016

DOI: 10.1039/c6lc00903d

www.rsc.org/loc

Introduction

Living cells are exposed to a complex and dynamic micro-mechanical environment. Looking at the circulatory system for instance, muscle contraction generates tensile and contractile stress in the tissues whereas blood and lymph flows generate shear stress. Long overlooked, the role of mechanics in cell regulation has become a very active field of research. It is now widely accepted that cells can sense and adapt to their mechanical environment, and that biochemical signals can similarly modify cells response to mechanical forces.^{1,2} Mechanical cues have been linked with fundamental cellular functions such as proliferation^{3–5} and differentiation,^{3,6} as well as with the development of numerous diseases including atherosclerosis⁷ and cancers.⁸ A better insight into cell

mechanobiology could lead to better diagnosis and treatments for some of the leading causes of death in the world including heart diseases and cancers, as well as provide valuable knowledge for other promising fields of research such as tissue engineering.

Due to the complexity of the *in vivo* environment, mechanical stimulation of cells is typically studied *in vitro*. To overcome the limitations of standard static culture dishes, techniques have been developed to apply mechanical loads on cultured cells. Experiments on individual cells have been used for the characterization of mechanical properties such as cell⁹ and membrane¹⁰ stiffness, and to study the dynamics of fast cellular responses such as the activation of mechanosensitive ion channels.^{11,12} More representative of the *in vivo* environment, experiments on cell populations have been used to study biological responses such as stretch-induced morphological changes^{3,13} and gene expression.³ Cell monolayers are used in most cases but there is growing interest in 3D cultures^{14,15} which provide better model of the *in vivo* environment.

Mechanical stimuli acting on cells can be described in terms of shear, tensile and compressive stress. Flow experiments based on a rocking platform¹⁶ or simple fluidic

^a Microsystems for Space Technologies Laboratory, Ecole Polytechnique Fédérale de Lausanne (EPFL), 2002 Neuchâtel, Switzerland.

E-mail: alexandre.poulin@epfl.ch

^b Vascular and Tumor Biology Laboratory, Department of Fundamental Oncology and Ludwig Institute for Cancer Research, Université de Lausanne (UNIL), 1066 Epalinges, Switzerland

† Electronic supplementary information (ESI) available. See DOI: 10.1039/c6lc00903d



systems¹⁷ are used to generate and study the effect of shear stress. Tensile and compressive stress on the other hand are more challenging to generate. Mechanical stimulation of single cells can be achieved using a wide range of technologies including atomic force microscope,¹⁰ microelectromechanical systems,¹⁸ optical tweezers⁹ and microfluidics.¹⁹ Techniques for mechanical stimulation of cell populations all relies on the same basic principle: cells are cultured on a stretchable substrate which can be actively deformed. The cell-to-substrate adhesion ensures that any mechanical deformation generated in the substrate is effectively transferred to the cells. The specificities of each technique reside in the actuation technology used to deform the culture substrate.

Commercial products such as the pneumatic system developed by Flexcell International Corporation, and the mechanical systems developed by Strex Inc. and CellScale are available. In addition, many miniaturized arrays of cell stretchers have been reported in recent years, most of them based on pneumatic actuation. In the simplest configuration, suspended membranes are located on top of pneumatic chambers, and deflect under positive or negative pressure, thus generating isotropic tensile strain in the membranes.^{20–22} To avoid the resulting out-of-plane displacement, which makes optical monitoring difficult, negative pressure and underlying posts can be used.²³ It is also possible to replace the pneumatic back-chamber by a set of side-chambers, a complex but clever configuration enabling in-plane anisotropic strain.²⁴ Alternative actuation mechanisms have also been reported, including the use of piezoelectrically actuated pins of a Braille display to deform suspended membranes,²⁵ temperature-responsive culture substrates such as hydrogels²⁶ or liquid crystal elastomer,²⁷ and a magnetically actuated polymer micropillar surface.²⁸

In this work we use dielectric elastomer actuators (DEAs) to apply tensile stress to cells *in vitro*. Fig. 1(a) presents the working principle of DEAs, which consist of an elastomer membrane sandwiched between two stretchable electrodes. To improve actuation strain, the membrane is placed under equibiaxial tensile stress, and attached to a rigid frame to hold the horizontal λ_x and vertical λ_y prestretch. When a voltage difference is applied, an electrostatic force is generated between the two electrodes, which compresses the membrane. Due to the elastomer incompressibility, the thickness reduction is accompanied by a lateral expansion.²⁹ The idea behind this work is that cells can be cultured on top of the DEA and deform with the actuator. Compared with alternative systems based on pneumatic or mechanical actuation, the simple electrical control of DEAs eliminates the need for bulky and complex sets of motors or pumps. We previously reported an array of miniaturized DEAs capable of generating large uniaxial strain, a design with great potential for applications in cell biology.³⁰ In this work, we present an improved design and for the first time, integrate a DEA system with living cells. We present a DEA-based deformable bioreactor compatible with standard cell culture protocols. The transparent device is also compatible with inverted microscopes

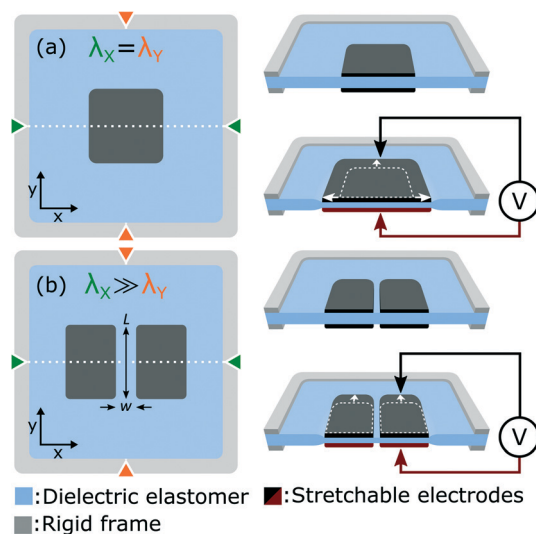


Fig. 1 (a) A DEA is composed of an elastomer membrane sandwiched between two stretchable electrodes. When a voltage difference is applied it generates electrostatic pressure on the membrane, which as a result decreases in thickness and expands laterally. A membrane under equibiaxial prestretch ($\lambda_x = \lambda_y$) undergoes equibiaxial actuation. (b) Uniaxial actuation is achieved by applying non-equibiaxial prestretch ($\lambda_x \gg \lambda_y$) on the membrane, effectively increasing the membrane stiffness along the high prestretch axis. Optical transparency is obtained using a gap of small aspect ratio (w/L) located at the center of the electrodes. This gap undergoes the same deformation as the bounding electrodes, providing large actuation strain in a highly transparent region of the actuator.

for real-time optical monitoring and fluorescence imaging. As a proof of concept, we cycled a population of lymphatic endothelial cells (LECs) between 0% and 10% uniaxial strain at a 0.1 Hz frequency during 24 h. Results show stretch-induced alignment and elongation of LECs, providing the first demonstration that DEAs can be interfaced with living cells and used to control their mechanical environment.

Materials and methods

The development of our DEA-based deformable bioreactor was guided by a set of fundamental requirements that we identified as indispensable: 1) the device and its materials have to be non-cytotoxic and compatible with standard cell culture protocols such as sterilization and incubation. 2) The system has to be compatible with inverted optical microscopes, and therefore optically transparent. 3) To cover the biologically relevant range of tensile strain levels, the device has to generate up to 20% uniaxial tensile strain. In this section we detail the design, materials, and protocols we developed and used to achieve those requirements.

Transparent uniaxial DEA design

The basic DEA design presented in Fig. 1(a) generates equibiaxial strain, whereas uniaxial strain is often more representative of the *in vivo* environment. Fig. 1(b) presents a slightly different design which provides uniaxial actuation



using non-equibiaxial prestretch ($\lambda_x \gg \lambda_y$). Due to the membrane hyperelastic properties, the prestretch anisotropy significantly stiffens the membrane along the X axis which results in preferential actuation along the Y axis. A small prestretch is still necessary along the Y axis in order to avoid loss of mechanical tension in the membrane during actuation.^{31–33} Uniaxial actuation strain as large as 80% was demonstrated using this prestretch configuration³⁰ on silicone-based DEAs.

The other important limitation of the design presented in Fig. 1(a) is that tensile strain is only generated in the electrode-covered area which is typically not transparent. While transparent stretchable electrodes have been reported, most DEAs relies on carbon-based materials which are highly absorbent in the visible range. For biological applications where cells are cultured on top of the actuator, non-transparent electrodes make real-time optical inspection impossible with a standard inverted optical microscope. Fig. 1(b) presents a slightly different design which includes a gap of small aspect ratio (w/L) located at the center of the electrodes. The width w of the gap is aligned with the high prestretch axis λ_x . This geometry ensures that the gap deforms uniformly with the bounding electrodes, generating large uniaxial tensile strain in a highly transparent region of the actuator.

DEA-based deformable bioreactor

Fig. 2 presents the deformable bioreactor we developed. The mechanically active element is a DEA composed of an elasto-

mer (Sylgard 186, Dow Corning) membrane under non-equibiaxial prestretch ($\lambda_x = 2.7$, $\lambda_y = 1.2$) sandwiched between two stretchable electrodes made of a carbon-back elastomer composite material.³⁴ The 30 μm thick membrane is fixed between two rigid plastic frames in order to maintain its prestretch. The frames also includes metallic electrical contacts which are pressed against the stretchable electrodes during assembly. The actuator design is the same as presented in Fig. 1(b) and therefore generates uniaxial tensile strain along the low prestretch λ_y axis. Uniaxial compressive strain can also be generated by simply rotating the design in order to have the gap length w aligned with the low prestretch axis instead.³⁵ The central gap between the electrodes is $w = 0.5$ mm wide by $L = 1.5$ mm long. The membrane dimension in the actuation direction is ten times larger than the electrodes width L which minimizes the effects of the fixed boundary condition.³²

The DEA is covered on both sides by a biocompatible elastomer (Silbione LSR4305, BlueStar Silicones) membrane. The main roles of this passivation is to differentiate the actuator requirements from the cell culture requirements, providing more flexibility in the choice of materials. The DEA membrane was selected for its combination of high dielectric strength and low Young's modulus, while the passivation was selected for its biocompatibility. Depending on the type of cells and the intended biological experiment, different passivation materials could be used such as an elastomer of higher Young's modulus to improve cell adhesion, a patterned membrane to induce cell organization, or a biological scaffold material. It is however important to consider that the passivation stiffening impact can limit the actuation strain, similarly to the stiffening impact of electrodes in the case of ultra-thin DEAs.^{36,37} Our passivation Young's modulus ($Y_{\text{pass}} = 0.2$ MPa) is 5 times lower, and its thickness ($t_{\text{pass}} = 2$ μm) is 15 times smaller than the DEA membrane ($Y_{\text{act}} = 1$ MPa, $t_{\text{act}} = 30$ μm), and therefore has a negligible stiffening impact on the device. Our ability to pattern very thin silicone membranes is a key advantage, which enables the use of stiffer materials ($Y_{\text{pass}} < 1$ MPa) without having to compromise on the actuation strain.

A 100 μm thick glass slide is mounted on the bottom rigid frame with the use of a 180 μm thick spacer. The interstice between the membrane and the glass slide is filled with saf-flower oil and the whole assembly is sealed. This oil encapsulation acts as a barrier between the cell culture and the surrounding environment. Control of CO_2 , humidity and temperature is consequently only required for the top chamber while the bottom side can be exposed to room environment. With a 310 μm gap between the cell culture and the bottom of the device, the deformable bioreactor can be easily mounted on top of an inverted microscope for *in situ* live cell imaging. While standard microscope objectives can be used for up to 20 \times magnification, long working distance objectives are required for higher magnification. The oil backing also help to stabilize the membrane vertical position. Its closed volume minimizes sagging effects and enables real-time

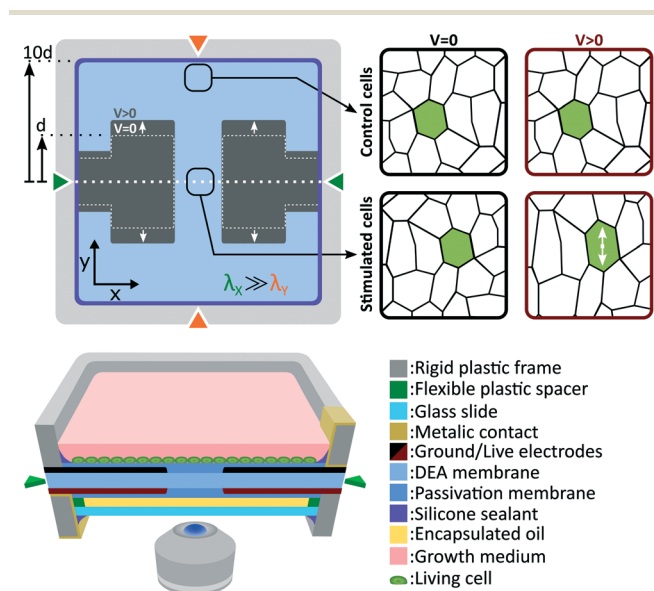


Fig. 2 Schematic diagram of the DEA-based deformable bioreactor. The cross-section shows a DEA composed of a silicone elastomer membrane sandwiched between two stretchable electrodes. The membrane is under non-equibiaxial prestretch and the actuator provides uniaxial tensile strain. The actuator is coated on both sides by a layer of biocompatible elastomer. The cell culture is located on top of the device, while an oil encapsulation protects the other side. Cells located at the gap and on the electrodes experience uniaxial tensile strain during actuation, whereas cells outside this region can be used as a static control population.



optical monitoring without complex feedback position control (more details can be found in the ESI†).

Cells are cultured the device top side, and immersed in cell growth medium. The culture chamber and the top electrode are grounded, whereas the bottom electrode is live. When actuated, the DEA generates uniform tensile strain on cells located at the gap and on the electrode. Due to the fixed boundary condition imposed by the rigid frames on the membrane, expansion of the active area induces contraction of the passive area. To minimize this effect, the membrane dimension along the actuation direction is set to 10 times the electrodes width d . This configuration ensures that compressive strain in the passive region is negligible compare to tensile strain in the active region. Cells located in the passive region of the membrane are consequently used as a static control population.

Actuation strain measurements

We measured the average strain generated in the gap by tracking changes of width Δw and length ΔL upon actuation, calculating strain along x as $\epsilon_{xx} = \Delta w/w$, and along y as $\epsilon_{yy} = \Delta L/L$. While this technique is simple to implement and gives a good evaluation of the device performance, it averages strain over the gap area, a measurement which can hide valuable information. For that reason, we also measured the strain profile over the gap area using digital image correlation (DIC). As previously reported,^{36,37} we used the device surface topography and DIC to map displacement upon actuation, and then calculated the corresponding strain field. The measured strain profiles can be found in the ESI.†

Cell preparation

The culture chamber of the DEA-based deformable bioreactor was incubated with fibronectin ($6 \mu\text{g cm}^{-2}$) in phosphate buffered saline (PBS) for 1 hour at room temperature to promote cell adhesion. The device was next filled with endothelial cell growth medium (Lonza) and incubated at 37°C for 24 h. Pre-conditioning of poly(dimethylsiloxane) in growth medium containing fetal bovine serum was reported to modify surface chemistry and significantly improve cell attachment.³⁸ Human lymphatic endothelial cells (LECs) were cultured as described previously,³⁹ and seeded on the fibronectin-coated device ($60\text{k cells per cm}^2$). A confluent LECs monolayer was obtained within 24 h of incubation at 37°C , 5% CO_2 and 95% relative humidity.

Mechanical stimulation of LECs

After reaching a confluent cell monolayer, the device was mounted on an inverted microscope as presented in Fig. 3. A portable incubator was used to control temperature, CO_2 and humidity levels in the culture chamber. An opening in the incubator provided optical access for the microscope objective, while the oil backing kept the cell culture isolated from the room environment. After the incubator reached equilibrium, the device was connected to a high-voltage power supply, and

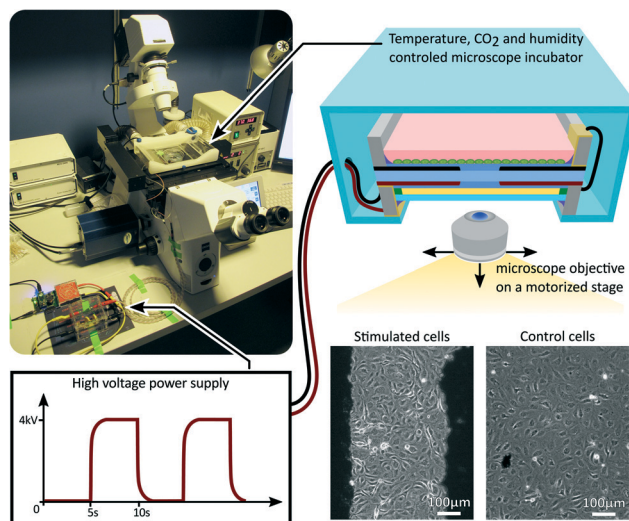


Fig. 3 The DEA-based deformable bioreactor was mounted on an inverted microscope during the stretching experiment. The microscope was programmed to periodically acquire pictures from different locations of the cell culture. A portable incubator was used to maintain the culture chamber at controlled temperature, CO_2 concentration and humidity level. The device was cycled between 0% and 10% uniaxial strain at a 0.1 Hz frequency with a 50% duty cycle for 24 h.

cycled between 0% and 10% uniaxial strain at a 0.1 Hz frequency with a 50% duty cycle for 24 h. A low-pass filter was connected between the power supply and the device in order to smooth the device driving signal. The filter had a cut-off frequency of 1 Hz, while the actuator has a cut-off frequency greater than 10 Hz, typical for silicone-based DEAs.⁴⁰ The strain level and frequency were selected to reproduce the mechanical environment of LECs in the lymphatic valves.⁴¹ While acute cell response can occur within the first few hours of mechanical stimulation, long term effect are often more representative of the *in vivo* environment. For that reason we designed a 24 h experiment, during which the microscope was programmed to periodically acquire pictures from different locations of the cell monolayer, monitoring the mechanically stimulated and static control areas of the device.

Effects of fringing electric field on LECs

When the electrodes of a DEA are completely overlapping as presented in Fig. 2, the electric field generated by the actuator is mostly confined within the membrane. Cells located at the border of the electrode are however not perfectly shielded. In order to confirm that morphological changes observed on LECs upon stretching are not induced by fringing electric field, we repeated the stretching experiment with an immobilized device. In order to suppress the actuation we replaced the oil backing by a glass slide directly bonded to the membrane. The cells on the immobilized device are exposed to the same electric field, while not being mechanically stimulated, effectively decoupling the electric field exposure from the mechanical stimulation. The results of this experiment



are summarized in the discussion section, and a more detailed analysis can be found in the ESI.†

Staining and microscopy

After stopping the mechanical stimulation, cells were fixed with a solution of 4% paraformaldehyde (Sigma-Aldrich) in PBS, permeabilized with 0.1% Triton X-100 (Applichem) and blocked with blocking buffer (0.5% BSA, 5% donkey serum, 0.01% sodium azide, 0.1% Triton X-100 in PBS). Phalloidin and Hoechst were diluted in blocking buffer as stated in product sheet and used to stain F-actin and deoxyribonucleic acid (DNA). Cells were incubated with this solution for 1 h at room temperature, washed with 0.1% Triton X-100 in PBS, and kept immersed in PBS. Fluorescence imaging was performed through the oil backing using a confocal Zeiss LSM 880 microscope with a 20× objective lens (Plan-Apochromat 20×/0.8 DIC M27 (WD = 0.55 mm)), and processed using Imaris software.

Evaluation of LECs morphology

Confocal microscope images obtained for F-actin and DNA staining were used to quantify cells morphology. Using ImageJ we calculated the alignment relative to stretch direction and the elongation of LECs. For each cell we determined a long axis and defined a perpendicular short axis. The orientation was calculated as the angle created (clockwise) between the stretch direction and the long axis. The elongation was calculated as the ratio between lengths of the long and short axis.

Results and discussion

The fabricated device is presented in Fig. 4(a). Stretchable electrodes appear in black on a transparent elastomer membrane, whereas the rigid frames used to hold prestretch and create a culture chamber appear in green with a silver pad for electrical connection. The average strain generated in the gap was measured by tracking the electrodes boundaries as described in Fig. 4(b). The actuation strain is presented in Fig. 4(c) as a function of the electric field applied across the membrane. The actuation strain is limited to $\epsilon_{yy} = 35\%$ by loss of mechanical tension, and not by electromechanical instability.^{31–33} An electric field of $130 \text{ V } \mu\text{m}^{-1}$, which corresponds to a driving voltage of 3.9 kV for a $30 \text{ } \mu\text{m}$ thick membrane, is required to reach $\epsilon_{yy} = 10\%$. The actuation is not perfectly uniaxial, and the tensile strain ($\epsilon_{yy} = 10\%$) is accompanied by a transversal compressive strain $\epsilon_{xx} = -2.5\%$, providing a strain ratio equal to $\epsilon_{yy}/\epsilon_{xx} = 4$.

Additional measurements were performed in order to show the strain uniformity in the gap area. Experimental measurements of ϵ_{xx} and ϵ_{yy} profiles are presented in the ESI.†

Fig. 5(a) and (b) presents fluorescence micrographs acquired in the stimulated and static control areas of the device, respectively. The measurements were made after 24 h of cyclic actuation between 0% and 10% strain at a 0.1 Hz fre-

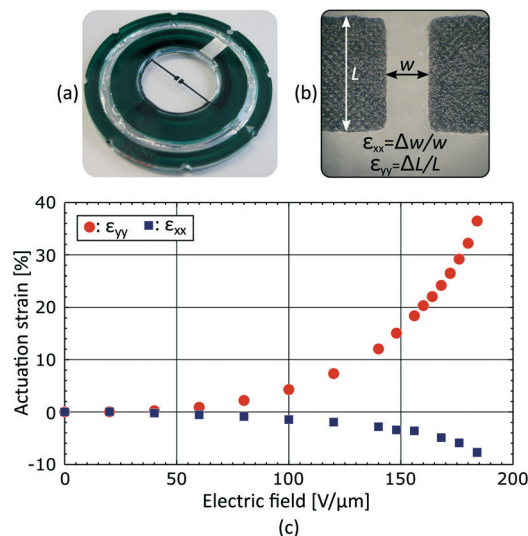


Fig. 4 (a) Picture of a fabricated DEA-based deformable bioreactor, where the stretchable electrodes appear in black, on a transparent membrane, held by a green rigid plastic frame. (b) Picture of the electrode gap, with the equations used to calculate the average strain generated in the gap upon actuation. (c) Average strain in the gap as a function of the electric field applied across the $30 \text{ } \mu\text{m}$ thick membrane. The actuation is limited to $\epsilon_{yy} = 35\%$ by loss of mechanical tension, and is accompanied by a transversal compression of $\epsilon_{xx} = -7.5\%$. At a driving voltage of 3.9 kV, the device reaches $\epsilon_{yy} = 10\%$ and $\epsilon_{xx} = -2.5\%$.

quency. The signal obtained from the DNA staining is shown in blue, while the signal obtained from the F-actin staining is shown in green. The DNA is concentrated in the nucleus and can be used to identify and count cells, whereas F-actin is particularly abundant beneath the cell membrane and can be used to characterize cells morphology. The results show that the cells in the stimulated region tend to be more elongated and to align perpendicular to the applied strain, while cells in the static control tend to have a random orientation.

We characterized cell morphology in the stimulated and static control areas. Fig. 5(a) presents the orientation distribution with respect to the strain axis. Green ellipses and black arrows on the left schematize cells and the strain axis respectively. Results show random distribution in the control area and preferential orientation around 100° in the stimulated area. Stretch-induce alignment has been reported for different types of cells² and is expected for LECs. The alignment is however typically perpendicular to strain which would corresponds to an orientation of 90° in Fig. 5. The strain axis is difficult to precisely identify when analysing the fluorescence micrographs, and the 10° offset is probably due to a misalignment of the sample during imaging. Fig. 5(b) presents the elongation distribution. The elongation coefficient corresponds to the ratio between the long and short axis of a cell, and the green ellipses on the left schematize the corresponding shapes. Results show that stimulated cells are more elongated, and based on cells orientation we can also conclude that elongation is perpendicular to the direction of strain.



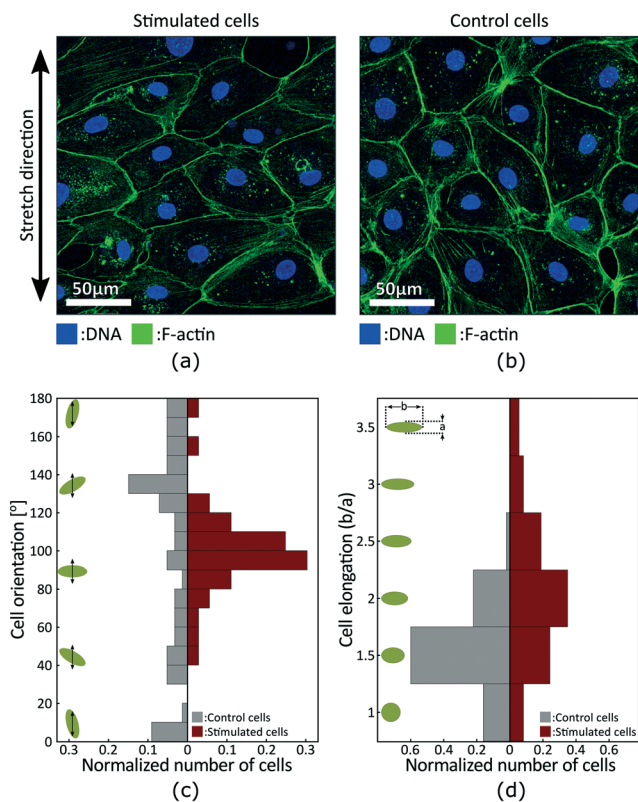


Fig. 5 Fluorescent micrographs acquired in the (a) stimulated and (b) static control areas show stretch-induced alignment of LECs. Measurements were done after 24 h of cyclic actuation between 0% and 10% strain at a 0.1 Hz frequency. (c) Orientation distribution of cells in the static control and stimulated areas. The green ellipses and the black arrows schematize the cells and the strain axis respectively. Results show stretch-induced alignment of LECs perpendicular to strain. (d) Elongation distribution of cells in the static control and stimulated areas. Elongation is calculated as the ratio between the long and short axis of cells, and the green ellipses schematize the corresponding cell shapes. Results show stretch-induced elongation of LECs.

The same stretching experiment was repeated with an immobilized device. In this configuration, cells were exposed to periodic electric field, without being exposed to mechanical stimulation. For the same applied electric field, the actuation strain was more than one order of magnitude lower on the immobilized device. This control experiment made it possible to decouple the effects of the device electric field, from the mechanical stimulation. The results showed no change in cells morphology, effectively demonstrating that the alignment and elongation of LECs reported in Fig. 5 was not stimulated by electric field, but induced by the periodic mechanical stimulation. The details of this control experiment can be found in the ESI†

In addition to LECs, we also cultured and stretched bronchial smooth muscle cells, fibroblasts, osteoblasts and cardiomyocytes. The device showed no visible effect on cell viability but strain rate was identified as a sensitive parameter. In some experiments, fast actuation of the device induced cell detachment and the driving signal had to be modified in order to limit strain rate. The fast response of DEAs can also

be an advantage over alternative technologies, providing the possibility to model extreme environments and look at the effect of head trauma on neurones for example.

Conclusion

We presented a DEA-based deformable bioreactor which can generate up to 35% uniaxial tensile strain on cells *in vitro*. Using DEAs we integrated the mechanically active element within the deformable culture substrate, providing a compact solution with a simple control system. The transparent device can be easily mounted on an inverted microscope for continuous optical monitoring of stimulated and control cell populations. As a proof of concept we cycled a monolayer of LECs between 0% and 10% uniaxial tensile strain at a 0.1 Hz frequency for 24 h. Using fluorescence imaging we analysed cells morphology in the stimulated and static control areas. Results showed stretch-induced alignment and elongation of LECs under uniaxial tensile strain, providing the first validation that DEAs can be interfaced with living cells and used to control their mechanical environment. We presented a practical approach for the development of a new generation of deformable bioreactors. The soft nature of DEAs and their great design flexibility are key advantages of this technology. While the presented device was developed for uniaxial tensile strain, the prestretch orientation can be modified to generate compressive or shear strain instead. In addition, a single membrane could integrate an array of independent actuators and test different mechanical stimuli in parallel.

Acknowledgements

This work was supported by the Swiss National Science Foundation (SNSF) under the grants 200020_153122 and 200020_165993, the SNSF R'equip program 206021_139187, and the People Programme (Marie Curie Actions) of the European Union's Seventh Framework Programme FP7/2007-2013/ under REA grant agreement 317250 to C. S. D.

References

- 1 G. Bao and S. Suresh, *Nat. Mater.*, 2003, **2**, 715–725.
- 2 J. H.-C. Wang and B. P. Thampatty, *Biomech. Model. Mechanobiol.*, 2006, **5**, 1–16.
- 3 T. M. Maul, D. W. Chew, A. Nieponice and D. A. Vorp, *Biomech. Model. Mechanobiol.*, 2011, **10**, 939–953.
- 4 A. Aryaei and A. C. Jayasuriya, *Mater. Sci. Eng., C*, 2015, **52**, 129–134.
- 5 Y. Gao, B. Zhou, X. Wu, X. Gao, X. Zeng, J. Xie, C. Wang, Z. Ye, J. Wan and W. Wen, *ACS Biomater. Sci. Eng.*, 2015, **2**, 65–72.
- 6 J. S. Park, J. S. F. Chu, C. Cheng, F. Chen, D. Chen and S. Li, *Biotechnol. Bioeng.*, 2004, **88**, 359–368.
- 7 D. M. Wootton and D. N. Ku, *Annu. Rev. Biomed. Eng.*, 1999, **1**, 299–329.
- 8 K. R. Levental, H. Yu, L. Kass, J. N. Lakins, M. Egeblad, J. T. Erler, S. F. T. Fong, K. Csiszar, A. Giaccia, W. Weninger, M.



- Yamauchi, D. L. Gasser and V. M. Weaver, *Cell*, 2009, **139**, 891–906.
- 9 G. Lenormand and A. Richert, *Biophys. J.*, 1999, **76**, 1145–1151.
 - 10 V. Lulevich, T. Zink, H.-Y. Chen, F.-T. Liu and G.-Y. Liu, *Langmuir*, 2006, **22**, 8151–8155.
 - 11 K. Svennersten, M. Berggren, A. Richter-Dahlfors and E. W. H. Jager, *Lab Chip*, 2011, **11**, 3287–3293.
 - 12 S. Schurmann, S. Wagner, S. Herlitze, C. Fischer, S. Gumbrecht, A. Wirth-Hucking, G. Prohl, L. A. Lautscham, B. Fabry, W. H. Goldmann, V. Nikolova-Krsteovski, B. Martinac and O. Friedrich, *Biosens. Bioelectron.*, 2016, **81**, 363–372.
 - 13 M. Morioka, H. Parameswaran, K. Naruse, M. Kondo, M. Sokabe, Y. Hasegawa, B. Suki and S. Ito, *PLoS One*, 2011, **6**, 1–9.
 - 14 C. Moraes, G. Wang, Y. Sun and C. A. Simmons, *Biomaterials*, 2010, **31**, 577–584.
 - 15 A. Gelmi, A. Cieslar-Pobuda, E. de Muinck, M. Los, M. Rafat and E. W. H. Jager, *Adv. Healthcare Mater.*, 2016, 1–10.
 - 16 R. P. Tucker, P. Henningsson, S. L. Franklin, D. Chen, Y. Ventikos, R. J. Bomphrey and M. S. Thompson, *J. R. Soc., Interface*, 2014, **11**, 20140330.
 - 17 B. Roy, T. Das, D. Mishra, T. K. Maiti and S. Chakraborty, *Integr. Biol.*, 2014, **6**, 289–299.
 - 18 D. B. Serrell, T. L. Oreskovic, A. J. Slifka, R. L. Mahajan and D. S. Finch, *Biomed. Microdevices*, 2007, **9**, 267–275.
 - 19 D. R. Gossett, H. T. K. Tse, S. A. Lee, Y. Ying, A. G. Lindgren, O. O. Yang, J. Rao, A. T. Clark and D. Di Carlo, *Proc. Natl. Acad. Sci. U. S. A.*, 2012, **109**, 7630–7635.
 - 20 Q. Wang, X. Zhang and Y. Zhao, *J. Micromech. Microeng.*, 2013, **23**, 015002.
 - 21 K. Shimizu, A. Shunori, K. Morimoto, M. Hashida and S. Konishi, *Sens. Actuators, B*, 2011, **156**, 486–493.
 - 22 F. Michielin, E. Serena, P. Pavan and N. Elvassore, *RSC Adv.*, 2015, **5**, 98429–98439.
 - 23 C. S. Simmons, J. Y. Sim, P. Baechtold, A. Gonzalez, C. Chung, N. Borghi and B. L. Pruitt, *J. Micromech. Microeng.*, 2011, **21**, 54016–54025.
 - 24 D. Tremblay, S. Chagnon-Lessard, M. Mirzaei, A. E. Pelling and M. Godin, *Biotechnol. Lett.*, 2014, **36**, 657–665.
 - 25 Y. Kamotani, T. Bersano-Begey, N. Kato, Y. C. Tung, D. Huh, J. W. Song and S. Takayama, *Biomaterials*, 2008, **29**, 2646–2655.
 - 26 D. Chen, R. D. Hyldahl and R. C. Hayward, *Lab Chip*, 2015, **15**, 1160–1167.
 - 27 A. Agrawal, O. Adetiba, H. Kim, H. Chen, J. G. Jacot and R. Verduzco, *J. Mater. Res.*, 2015, **30**, 453–462.
 - 28 F. Khademolhosseini, *Biomed. Microdevices*, 2016, 1–11.
 - 29 R. Pelrine, *Science*, 2000, **287**, 836–839.
 - 30 S. Akbari and H. R. Shea, *Sens. Actuators, A*, 2012, **186**, 236–241.
 - 31 M. Kolloosche, J. Zhu, Z. Suo and G. Kofod, *Phys. Rev. E: Stat., Nonlinear, Soft Matter Phys.*, 2012, **85**, 2–5.
 - 32 S. J. A. Koh, T. Li, J. Zhou, X. Zhao, W. Hong, J. Zhu and Z. Suo, *J. Polym. Sci., Part B: Polym. Phys.*, 2011, **49**, 504–515.
 - 33 X. Zhao and Z. Suo, *Phys. Rev. Lett.*, 2010, **104**, 1–4.
 - 34 S. Rosset, S. Araromi, S. Schlatter and H. Shea, *J. Visualized Exp.*, 2016, **108**, 231–238.
 - 35 A. Poulin, S. Rosset and H. Shea, Electroactive Polymer Actuators and Devices (EAPAD), *Proc. SPIE*, 2014, **9056**, 90561Q.
 - 36 A. Poulin, S. Rosset and H. R. Shea, *Appl. Phys. Lett.*, 2015, **107**, 244104.
 - 37 A. Poulin, S. Rosset and H. Shea, Electroactive Polymer Actuators and Devices (EAPAD) 2016, *Proc. SPIE*, 2016, **9798**, 97980L.
 - 38 L. Wang, B. Sun, K. S. Ziemer, G. A. Barabino and R. L. Carrier, *J. Biomed. Mater. Res., Part A*, 2010, **93**, 1260–1271.
 - 39 C. Norrmen, W. Vandeveld, A. Ny, P. Saharinen, M. Gentile, G. Haraldsen, P. Puolakkainen, E. Lukanidin, M. Dewerchin, K. Alitalo and T. V. Petrova, *Blood*, 2010, **115**, 906–909.
 - 40 S. Rosset, P. Gebbers, B. M. O'Brien and H. R. Shea, *Proc. SPIE*, 2012, 834004.
 - 41 K. N. Margaritis and R. A. Black, *J. R. Soc., Interface*, 2012, **9**, 601–612.

